Monthly Notices of the ROYAL ASTRONOMICAL SOCIETY

MNRAS **518,** 5403–5413 (2023) https://doi.org/10.1093/mnras/stac3371
Advance Access publication 2022 November 24

No memory of past warps in the vertical density structure of galaxies

Joaquín García de la Cruz [1,2]★ Marie Martig[1]★ and Ivan Minchev [3]

[1]*Astrophysics Research Institute, Liverpool John Moores University, 146 Brownlow Hill, Liverpool L3 5RF, UK*
[2]*Institut de Ciències del Cosmos (ICCUB), Universitat de Barcelona (IEEC-UB), Martí i Franquès 1, E-08028 Barcelona, Spain*
[3]*Leibniz-Institut für Astrophysik Potsdam (AIP), An der Sternwarte 16, D-14482, Potsdam, Germany*

Accepted 2022 November 7. Received 2022 October 22; in original form 2021 November 2

ABSTRACT

Warps are observed in a large fraction of disc galaxies, and can be due to a large number of different processes. Some of these processes might also cause vertical heating and flaring. Using a sample of galaxies simulated in their cosmological context, we study the connection between warping and disc heating. We analyse the vertical stellar density structure within warped stellar discs, and monitor the evolution of the scale heights of the mono-age populations and the geometrical thin and thick disc during the warp's lifetime. We also compare the overall thickness and the vertical velocity dispersion in the disc before and after the warp. We find that for warps made of pre-existing stellar particles shifted off-plane, the scale heights do not change within the disc's warped region: discs bend rigidly. For warps made of off-plane new stellar material (either born *in situ* or accreted), the warped region of the disc is not well described by a double sech^2 density profile. Yet, once the warp is gone, the thin and thick disc structure is recovered, with their scale heights following the same trends as in the region that was never warped. Finally, we find that the overall thickness and vertical velocity dispersion do not increase during a warp, regardless of the warp's origin. This holds even for warps triggered by interactions with satellites, which cause disc heating but before the warp forms. Our findings suggest that the vertical structure of galaxies does not hold any memory of past warps.

Key words: methods: numerical – galaxies: disc – galaxies: evolution – galaxies: interactions – galaxies: spiral – galaxies: structure.

1 INTRODUCTION

Warps in stellar disc of galaxies were first discovered by Van Der Kruit & Searle (1981). Large surveys of galaxies have since then shown that stellar warps are present in 40 per cent to 75 per cent of galaxies, depending on the nature of the sample (Reshetnikov & Combes 1998; Ann & Park 2006). Schwarzkopf & Dettmar (2001) even found that 93 per cent of interacting/merging galaxies present warps (versus 45 per cent of the non-interacting galaxies). Warps are also commonly observed in the H I disc of galaxies (Sancisi 1976; Bosma 1981; Heald et al. 2011). Small-scale bending waves or corrugation patterns have also been observed using dust lanes (e.g. Narayan, Dettmar & Saha 2020), and line-of-sight velocity fields (e.g. Alfaro et al. 2001; Sánchez-Gil, Alfaro & Pérez 2015; Gómez et al. 2021; Urrejola-Mora et al. 2022). Stellar warps reach amplitudes up to 25° (Sánchez-Saavedra et al. 2003), and gas warps amplitudes up to 33° (García-Ruiz, Sancisi & Kuijken 2002). The duration of warps is difficult to establish from observations, but simulations have found that warps can last from several Myr (Semczuk et al. 2020) to several Gyr (Shen & Sellwood 2006), depending on their formation mechanism. Different formation processes can also explain many of the warps' morphological properties (Saha & Jog 2006), for instance, whether warps are L-shaped (one-sided), S-shaped (one side of the disc rises, the other declines), or U-shaped (both sides of the disc rise/decline) (Kim et al. 2014).

In the Milky Way (MW), an H I warp has been detected at galactocentric radii larger than $R \sim 10$ kpc, reaching a height ∼4 kpc above the mid-plane in the North ($l \sim 90°$) and curving to the South ($l \sim 270°$) below 1 kpc (Levine, Blitz & Heiles 2006). A warp in the stellar Galactic disc has also been detected at galactocentric radii larger than $R \sim 9$ kpc, reaching heights above the mid-plane up to ∼5 kpc (e.g. López-Corredoira & Molgó 2014; Liu, Tian & Wan 2016; Poggio et al. 2018; Romero-Gómez et al. 2019; Cheng et al. 2020; Antoja et al. 2021). Simulations suggest that the warp in the Galactic disc is probably due to the gravitational influence of the infall of the Large Magellanic Cloud (Laporte et al. 2018, 2019; Poggio et al. 2021) or to the last passage through the Galactic disc of the Sagittarius dwarf galaxy with the Large Magellanic Cloud boosting the warp's amplitude (e.g. Purcell et al. 2011; Gómez et al. 2013; Antoja et al. 2018; Laporte et al. 2018, 2019; Hunt et al. 2021).

While Van Der Kruit (2007), using the SDSS survey, suggested that stellar and gaseous warps are different components, with different evolution scenarios, Gómez et al. (2017) found in simulations that gas and stars in warps follow the same pattern, and that they remain coincident for at least 1 Gyr. This seems to be in agreement with what Chen et al. (2019) found in the MW, where the morphology of the warp for the gas and the youngest stellar populations trace each other up to at least 20 kpc, suggesting that the two components are closely linked to each other.

Many mechanisms have been proposed for warp formation, including misalignment between the disc and the halo (Debattista &

★ E-mail: garciadlcruz@gmail.com (JGdlC); M.Martig@ljmu.ac.uk (MM)

Sellwood 1999; Ideta et al. 2000), misalignment between the inner stellar disc and the gas disc (Roškar et al. 2010; Aumer & White 2013), interactions between magnetic fields and HI gas (Battaner, Florido & Sanchez-Saavedra 1990; Battaner & Jiménez-Vicente 1998), accretion of intergalactic matter on to the disc (López-Corredoira et al. 2002; Semczuk et al. 2020), bending modes or waves embedded in the disc (e.g. Sparke & Casertano 1988; Revaz & Pfenniger 2004; Chequers & Widrow 2017), dark matter overdensity wakes (e.g. Weinberg 1998; Weinberg & Blitz 2006; Gómez et al. 2017; Laporte et al. 2018; Garavito-Camargo et al. 2019), and the gravitational interaction of an in-falling satellite (Ostriker & Binney 1989; Weinberg 1998; Jiang & Binney 1999). In the latter scenario, new infalls can regenerate and maintain the warp for several Gyr (Shen & Sellwood 2006).

Many of these mechanisms are often associated with disc heating and flaring (e.g. Gerssen & Shapiro Griffin 2012; Minchev et al. 2015; Pinna et al. 2018). For instance, mergers have been proposed to create disc heating (Toth & Ostriker 1992; Sellwood, Nelson & Tremaine 1998; Kazantzidis et al. 2008, 2009) and disc flaring (e.g. Villalobos & Helmi 2008; Bournaud, Elmegreen & Martig 2009; Martig, Minchev & Flynn 2014). Another example is misaligned infall of gas, which can also cause disc heating and flaring (Scannapieco et al. 2009), as well as warping. Therefore, disc heating and warping may happen simultaneously. Indeed, the outskirts of the MW's disc seem to be both flaring (e.g. Amôres, Robin & Reylé 2017; López-Corredoira et al. 2018; Thomas et al. 2018; Yu et al. 2021) and warping (e.g. Chen et al. 2019). Khachaturyants, Beraldo e Silva & Debattista (2021) suggested that settled warp stars may contribute to the flaring of the youngest stellar populations observed at large galactocentric radii in the MW. In some cases, it could even be possible that the warps themselves might directly cause some vertical heating: bending waves, a phenomenon closely related to warping, have been proposed to heat discs (Khoperskov et al. 2010; Griv 2011). However, heating and warping do not necessarily always happen together. In the case of satellite–galaxy interactions, whether the disc tilts or gets heated depends on different properties of the satellite, including its orbital properties (Velázquez & White 1999). Shen & Sellwood (2006) similarly found in simulations that in a satellite–galaxy interaction, the host galaxy's disc tilts remarkably rigidly, so that vertical heating is very limited.

Thus, it is worth exploring the connection between warping and disc heating/flaring. In this paper, we use a sample of simulated galaxies from Martig et al. (2012) to explore how much disc vertical heating happens during warps, and how warps affect the vertical stellar density structure of galactic discs. The paper is divided as follows: in Section 2, we describe the suite of simulations used as well as our methods to characterize the warps and the vertical structure of discs. In Section 3, we describe different properties of the warps, including how they form. In Section 4, we address the connection between warps, disc heating, and disc flaring; and summarize our conclusions in Section 5.

2 METHODS

2.1 Simulations

The simulations used in this work belong to a suite of simulated galaxies in their cosmological context from Martig et al. (2012). The technique employed in these simulations is described in more detail in Martig et al. (2009), and consists of two different stages. First, a dark-matter-only Λ cold dark matter cosmological simulation is performed with 512^3 dark matter particles. This is done using the adaptive mesh refinement code RAMSES (Teyssier 2002). In this simulation, we identify the dark matter haloes with a final mass between 2.7×10^{11} and 2×10^{12} $M_\odot$ that live in isolated environments. The merger histories and diffuse dark matter accretion are recorded for those haloes from $z = 5$ to $z = 0$. Secondly, a re-simulation follows the growth of a seed galaxy which evolves from $z = 5$ to $z = 0$ using the merger and accretion histories obtained in the first simulation. A galaxy containing stars, gas, and dark matter replaces each incoming halo. For this simulation stage, a Particle-Mesh code (Bournaud & Combes 2002, 2003) is used, where gas dynamics is modelled with a sticky-particle algorithm. Each simulation box is $800 \times 800 \times 800$ kpc in size, and the mass resolution is 1.5×10^4 $M_\odot$ for gas particles and stellar particles formed during the simulation, 7.5×10^4 $M_\odot$ for stellar particles in the initial seed galaxies at $z = 5$, and 3×10^5 $M_\odot$ for dark matter particles. The spatial resolution is 150 pc. Star formation obeys a Schmidt–Kennicutt law with an exponent of 1.5 (Kennicutt 1998) above gas densities of 0.03 $M_\odot$ pc^{-3}. Energy feedback from supernovae is included and a mass-loss scheme is implemented following that of Jungwiert, Combes & Palous (2001) and used in Martig & Bournaud (2010).

2.2 Warp selection and characterization

2.2.1 *Alignment of the galactic plane*

In order to study warps, we need to globally align the galactic disc in the XY plane. For this, we first compute the total angular momentum of all stellar particles inside a sphere of radius 20 kpc. We then rotate all particles to align this angular momentum with the Z axis. To refine the alignment of the disc in the XY plane, we rotate the disc a second time by computing again the total angular momentum's direction but, this time, within a cylinder with radius equal to R_{25} and height equal to six times the estimated disc thickness $h_{\rm scale}$. This estimated disc thickness is defined as the standard deviation of the vertical position of stars located at half the optical radius of the galaxy, R_{25}, also used and described in García de la Cruz et al. (2021).

For galaxies with a warped disc, after computing a first approximate warp onset radius (see next paragraphs), we rotate the disc a final time using only particles within the central unwarped region, and then recompute all warp parameters.

2.2.2 *Identifying warps*

After we ensure the discs are properly aligned with the XY plane, we create maps of the mean vertical position of stellar particles, and use those maps to visually identify the presence of warps. We consider that a disc is warped when an azimuthally wide area of the outer disc is off-plane (see examples in Fig. 1). We only select warps that clearly start within R_{25}. The identification of warps is done purely by visual inspection of the maps, and is a way to identify when the warps start to be fully developed: small perturbations might have started to grow before then. We track each galaxy as a function of time, and note when warps start and end. We consider a warp ends when the warped region of the disc is not longer shifted off-plane (again, based on a visual inspection of the maps). Our final sample consists of 11 warps: five that have ended by redshift $z = 0$ and six that are still ongoing.

2.2.3 *Characterizing warps*

Once we have identified the snapshots where the galactic disc is warped, we proceed to characterize the warps. For that, we divide

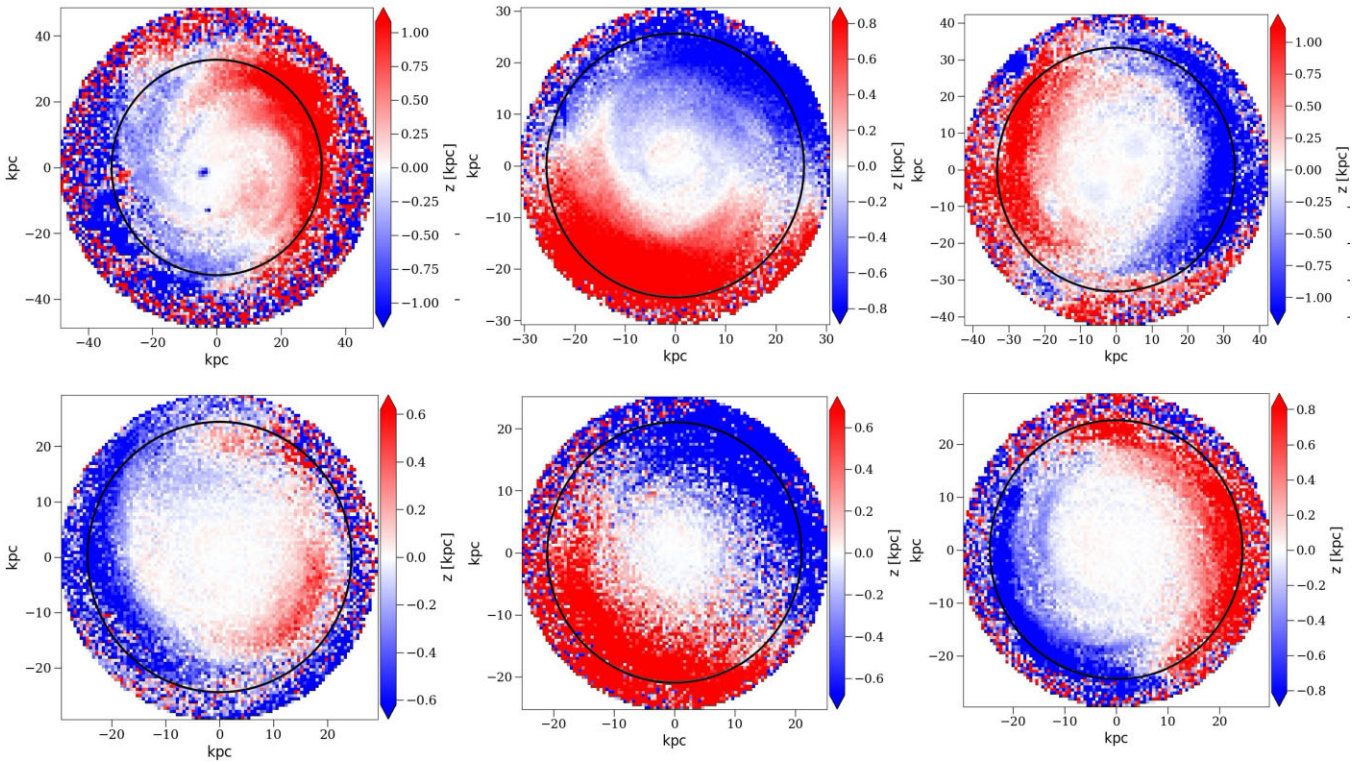

Figure 1. A sample of vertical position maps where warps are detected. From left to right and top to bottom: **g38**, **g83**, **g39**, **g62**, **g126**, and **g48**. Each pixel is colour-coded by the stellar particles' mean vertical position of stellar particles (note the different colour scales on each panel). The black circle corresponds to R_{25}, which we use to define the edge of the disc. The left column shows two examples of L-shaped warps (or one-sided), while the rest shows S-shaped warps (or two-sided).

the disc into 10 azimuthal sectors, and each sector into overlapping radial bins 2 kpc wide every 0.5 kpc. For each of these azimuthal and radial sectors, we bin the stellar particles into 100 vertical bins up to five times $h_{\rm scale}$ above and below the galactic plane, and identify the peak of the vertical density (the high number of bins ensures that we can precisely identify the position of the density peak). An example of this can be seen in Fig. 2.

We compute the maximum height above the mid-plane reached by the warp. We also compute the angle between the galactic plane and a line joining the maximum of the warp to the galactic centre: we will call this the warp angle.

From all the information extracted in this process and represented in Fig. 2, we also extract the onset radius of the warp, as it can clearly be seen when the peak of the vertical stellar density starts to shift away from the galactic plane. We record the value of the warp angle, height, and onset radius throughout the warp's life. The maximum values of the warp angle and height over its whole lifetime are found in Table 1.

2.3 Vertical density profiles and scale heights

We analyse the vertical density distribution for stars in the disc both inside and outside the warped region of the disc. To compute a single vertical density profile at a given radius, we first need to correct for the different vertical shifts in vertical density as a function of azimuth caused by the warp itself. For that, after dividing the disc into different azimuthal and radial bins as described in Section 2.2, we compute the dispersion of the vertical position of the stars in every disc region. Then, we compute the median value of the vertical position from all stellar particles whose vertical position is smaller

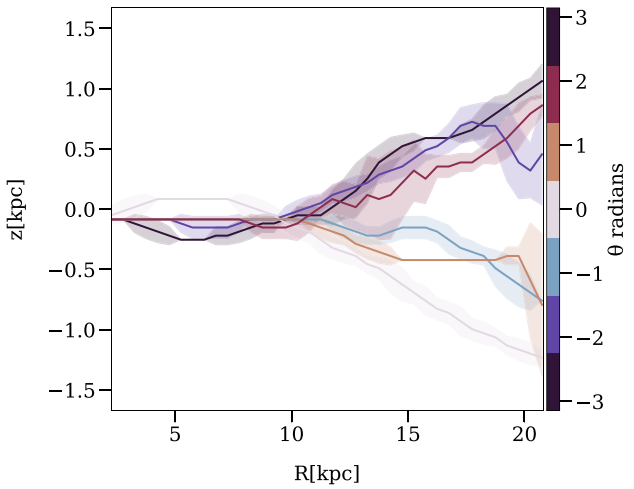

Figure 2. Mean vertical position of the stellar density peak as a function of radius colour-coded for different azimuthal angles for galaxy **g126**. The shaded areas represent the dispersion around the mean vertical position. The values at the largest radius are used to compute the maximum warp height and angle given in Table 1. We define the onset radius of the warp as the radius where the vertical position of the stars starts deviating from 0 for different azimuthal angles (this would be ∼11 kpc for galaxy **g126** shown here).

than the previously computed vertical dispersion. Finally, we shift uniformly all the stellar particles within the region by this median value. With this, the peak of the vertical stellar density is aligned

Table 1. Summary of the general features of our warp sample. In the final time column, the symbol '-' means the warp is ongoing by $z = 0$. In the symmetry/shape column, 'L' means the warp is one-sided, while 'S' means is two-sided, with each side going in opposite directions.

Galaxy ID	R_{25} at final time kpc	Initial time Gyr	Final time Gyr	Symmetry/shape	max. |z| kpc	max. $\|\theta\|$ °	Likely warp agent
g38	34.5	11.9	12.4	L	1.44	2.52	internally driven
g128	17.0	9.8	10.1	L	0.65	2.23	internally driven
g35	29.3	13.1	–	L	3.64	7.25	satellite
g62	24.4	13.0	–	S	1.60	3.72	satellite
g83	25.6	12.3	–	S	2.14	4.79	satellite
g126	21.0	12.1	–	S	2.00	5.47	satellite
g148	14.9	11.9	13.3	S	1.27	4.47	satellite
g48	24.7	9.8	–	S	5.20	11.91	stellar ring
g59	29.9	11.1	–	S	7.60	20.37	stellar ring
g102	21.5	9.8	12.6	S	2.78	8.60	stellar ring
g39	32.8	8.0	9.7	S	6.68	11.52	accretion

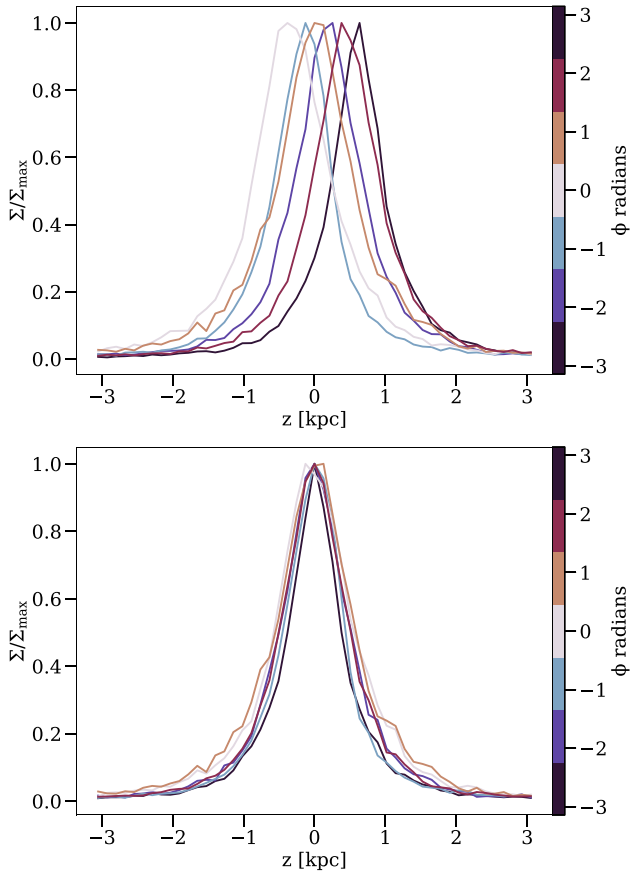

Figure 3. *Top:* normalized vertical stellar density for different azimuthal angles within a stellar ring in the disc for galaxy **g83**. *Bottom:* the result of shifting uniformly all stellar particles in the given azimuthal angle following the method described in Section 3. This shows density profiles that are very similar in the different angular sectors of the disc, with only small variations at large height. We apply this methodology for all the analysis of this work.

with the galactic plane of the galaxy for a given radius and azimuthal sector. An example of this technique is shown in Fig. 3.

After correcting for the vertical shift caused by the warp in different azimuthal sectors, we fit the density profiles with a double sech^2 representing a thin and thick disc following the same method as in García de la Cruz et al. (2021) and explained below. We bin the disc stellar particles in cylindrical shells with a width of 2 kpc and a height of 6 h_{scale}. At each radius, we compute the vertical number density of particles using 30 bins, and fit the profile using a combination of two sech^2 functions:

$$N(z) = N_0 \left((1-\alpha)\mathrm{sech}^2\left(\frac{z}{h_{\mathrm{thin}}}\right) + \alpha \mathrm{sech}^2\left(\frac{z}{h_{\mathrm{Thick}}}\right)\right), \quad (1)$$

where N_0 is the stellar number density at the mid-plane, h_{thin} and h_{Thick} correspond to the scale heights of the thin and thick disc respectively, and α is the number density fraction of the thick disc over the global disc.

The fits for the scale height are obtained using the Markov Chain Monte Carlo (MCMC) `python` package `EMCEE` (Foreman-Mackey et al. 2013) to sample the posterior distribution. Following Bennett & Bovy (2019), we use a Poisson distribution for the likelihood, which we write as follows:

$$\ln\mathcal{L}(N_c|N_p) = \sum -N_p + N_c \cdot \ln(N_p) - \ln(N_c!), \quad (2)$$

where N_c is the number of stellar particles counted in the bin, N_p is the number of stellar particles predicted by the model, and $N_c!$ is independent of the models and thus ignored for the computation of the likelihood. As for the priors, we let h_{thin} and h_{Thick} take any value from 0 to 15 kpc, α from 0 to 1, and we set N_0 to be positive.

We sample the posterior using 200 walkers and 5000 steps. The walkers start from random positions around the best-fitting value obtained using the `ScyPy` routine `curve_fit` (Virtanen et al. 2020). The final values we report for each parameter are the median and the 16th to 84th percentiles range of the posterior distribution.

We also compute the scale heights of mono-age populations by fitting a single sech^2 as discussed in García de la Cruz et al. (2021). The mono-age populations are obtained by splitting the stellar particles into 0.5 Gyr age bins from 0 to 9 Gyr, and 2 Gyr age bins from 9 to 13 Gyr. The spatial bins are the same used for the fits of the global thin and thick discs.

3 WARP FORMATION PROCESSES AND CHARACTERISTICS

After identifying and characterizing the galactic warps as described in Section 2, our final sample consists of 11 warps: five that have ended by redshift $z = 0$ and six that are still ongoing. In this section, we first present the mechanisms creating the warps, and then discuss the shape, duration, and amplitude of the warps.

We find that the different warp formation processes can be grouped into two categories. Warps belonging to the first group arise when the stellar particles living in the disc experience a shift of their vertical

position. In order words, the warp is made of stellar particles that already existed in the disc prior to the warp itself. The two main channels to create such a warp are vertical instabilities in the absence of satellite galaxies or through an interaction with a satellite galaxy, i.e. a flyby or a merger. On the other hand, warps belonging to the second group form when new stellar material is added to the galaxy in off-plane orbital configurations. This can happen either because stars are accreted on to the disc, or because stars are born already in an off-plane configuration out of a bent gas disc. Next, we provide a more detailed description of the formation of the warps from our sample (see also a summary in Table 1).

3.1 Internally driven warps

In two galaxies, we notice warps that appear while no massive satellite is visible in our stellar density maps (out to a distance of 80 kpc from the galactic centre). In those discs, a bending wave starts expanding from the inner disc outwards. When this bending wave reaches the outermost part of the disc, it has widened enough to form an L-shaped warp. The origin of this feature is difficult to determine. It could be related to the underlying dark matter distribution (e.g. Vesperini & Weinberg 2000; Weinberg & Blitz 2006; Gómez et al. 2017; Laporte et al. 2018), but we inspected the dark matter density maps and found no massive satellites orbiting around the galaxy. These warps might instead be triggered by the shape of the halo (Yurin & Springel 2015), by misalignments between the dark matter and the stellar component (Debattista & Sellwood 1999; Jiang & Binney 1999; Shen & Sellwood 2006), as well as by spiral arms (Faure, Siebert & Famaey 2014) or internal bending instabilities (Revaz & Pfenniger 2004). Given that this paper is mostly focused on how the vertical structure of discs responds to warps, rather that what caused the warps in the first place, we leave a full exploration of the origin of these warps for future work. We find two warps belonging to this category: **g38**, **g128**.

3.2 Interactions with satellites

These warps are created by the interaction between a satellite and the host galaxy, either a merger or a flyby (we list next the stellar masses of the satellites at their last apocentre before the encounter creating the warp). Galaxies belonging to this category mostly form S-shaped warps.

g35: a satellite with $M_\star = 6 \times 10^9\,M_\odot$ (corresponding to a mass ratio of 1:22 with respect to the stellar mass of the host galaxy) orbits several times around the galaxy. After a pericentre passage at $t \sim 12.9$ Gyr during which the satellite crosses the disc (at a distance of 14 kpc from the centre), a warp appears at $t \sim 13.1$ Gyr on the side of the disc through which the satellite has passed (this is the only L-shaped warp of this category).

g62: a satellite with $M_\star = 2 \times 10^9\,M_\odot$ (corresponding to a mass ratio of 1:27) crosses the disc at $t \sim 11.8$ Gyr. This crossing coincides with its pericentre passage (16 kpc from the centre of the galaxy) and creates multiple vertical bending waves. Around $t \sim 13.0$ Gyr, a warp develops on one side of the disc and then shortly evolves into an S-shaped warp.

g83: a satellite with $M_\star = 1.9 \times 10^9\,M_\odot$ (corresponding to a mass ratio of 1:21) orbits the disc in a highly inclined configuration. It reaches its first pericentre (28 kpc from the centre) at 11.4 Gyr, creating a warp at $t \sim 12.3$ Gyr. A second passage at $t \sim 13.4$ Gyr increases the amplitude of the warp.

g148: a satellite with $M_\star = 4 \times 10^8\,M_\odot$ (corresponding to a mass ratio of 1:70) orbits the disc with a low inclination. A pericentre passage at 10.9 Gyr (14 kpc from the centre) triggers a warp at $t \sim 11.9$ Gyr.

g126: a satellite with $M_\star = 3 \times 10^9\,M_\odot$ (corresponding to a mass ratio of 1:8) orbits the disc with a low inclination before merging with the core of the galaxy at 11.2 Gyr. The interaction creates vertical oscillations propagating from the inner to the outer disc. The warp forms at $t \sim 12.1$ Gyr when these vertical oscillations reach the outer disc. A stellar ring forms later on, at $t \sim 12.5$ Gyr, in a slightly bent configuration, which reinforces the warp and increases its duration.

3.3 Accretion on an inclined orbit

g39: a satellite with $M_\star = 7 \times 10^9\,M_\odot$ (corresponding to a mass ratio of 1:18) orbits the disc a few times before merging with the core of the galaxy at 8 Gyr. During its final inspiral (starting at 7.5 Gyr) the satellite scatters around stellar particles both belonging to the satellite and the host galaxy in off-plane configurations. At $t \sim 8$ Gyr, the disc grows and the off-plane material falls back on to the disc, forming an S-shaped warp.

3.4 Formation of an inclined stellar ring

These warps form when a massive merger perturbs the gas disc, which ends up misaligned with respect to the stellar disc. Later on, a flyby triggers star formation in the outer regions of the inclined gas disc, forming an inclined stellar ring. The gravitational interaction between the stellar disc and the stellar ring pulls the latter down to the galactic plane. The warp is the product of this mixing between the aligned stellar disc and the off-plane stellar material. As with warps created from interactions with satellites, these warps are also S-shaped. A visual representation of this process can be found in Appendix A.

g48: a satellite with $M_\star = 1.1 \times 10^{10}\,M_\odot$ (corresponding to a mass ratio of 1:4) merges with the core of the galaxy at 8.2 Gyr. About 1.5 Gyr later, at $t \sim 9.8$ Gyr, a stellar ring forms following a flyby from another satellite. The time evolution of this galaxy is shown in Appendix A.

g59: a satellite with $M_\star = 1 \times 10^{10}\,M_\odot$ (corresponding to a mass ratio of 1:3) merges with the core of the galaxy at 8.3 Gyr. Its final inspiral starts at 7.5 Gyr, and spreads gas around the galaxy. During the next Gyr, flybys from two massive satellites keep the gas inclined until, finally, it condenses and forms stars at $t \sim 11.1$ Gyr. A stellar ring forms in an inclined configuration, and as with **g48**, this stellar ring creates the warp.

g102: a satellite with $M_\star = 1.5 \times 10^9\,M_\odot$ (corresponding to a mass ratio of 1:15) starts its final inspiral at 8 Gyr and merges with the core of the galaxy at 8.7 Gyr. In the next Gyr, two satellites pass close to the disc and, shortly after this, an inclined stellar ring develops outside of R_{25} at $t \sim 9.8$ Gyr. This structure progressively falls on to the disc, creating the warp.

We record the shape and duration of all these warps. We also compute the maximum height above the mid-plane reached by the warp as well as the maximum warp angle. All these properties are summarized in Table 1. The values we find for most warp angles are comparable to those found in observations (e.g. Sánchez-Saavedra et al. 2003; Ann & Park 2006; Reshetnikov et al. 2016) and in other simulations (e.g. Gómez et al. 2017). Only one galaxy, **g59**, is a clear outlier with a very strong warp when compared with observational studies. Such strong warps are rarely observed, but they exists (see e.g. Sánchez-Saavedra et al. 2003), and are not rare in simulations (Kim et al. 2014).

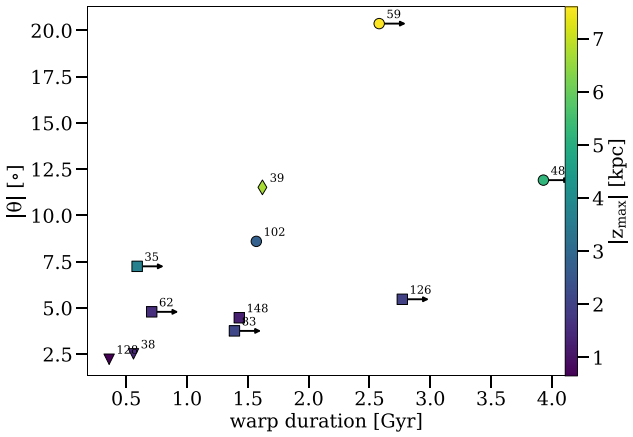

Figure 4. Maximum warp angle as a function of the duration of the warp, colour-coded by the maximum height over the galactic plane. The shape of points represents the origin of the warp: triangles are internally driven, squares are satellite interactions, diamonds are stellar accretion from inclined orbits, and circles are stellar rings being born in off-plane configurations.

In Fig. 4, we show the warp angle as a function of warp duration (the symbols indicate the origin of the warp, and the colour code the maximum height in kpc reached by the warp). For warps that are ongoing at $z = 0$ (indicated by an arrow), the measured duration is only a lower limit, but we still find a general correlations between warp amplitude and duration. We find that internally driven warps have the shortest duration, around 0.5 Gyr. Their maximum amplitudes are also the smallest within the sample, not reaching above $\sim 2.5^\circ$ (for **g38**, the warp reaches a maximum height of 1.4 kpc, which might seem high, but the optical radius of the galaxy is very large so that it corresponds to a small warp angle). By contrast, warps driven by gravitational interactions between satellites and their host galaxies (flybys or mergers) can last longer than 1 Gyr, in agreement with Shen & Sellwood (2006). The longest warp within this category is found in **g126**: as described earlier, this is a special case where the warp is reinforced by the creation of an inclined stellar ring. Compared to internally driven warps, warps created by interactions reach higher angles above the mid-plane, up to $\sim 7.2^\circ$. This general trend was also observed by Schwarzkopf & Dettmar (2001). Finally, warps produced by off-plane stellar rings or by off-plane stellar accretion have the longest duration within the sample, lasting several Gyr. These warps also reach the largest heights above the galactic plane.

4 MONITORING DISC HEATING DURING WARPS

In this section, we examine the evolution of the vertical density structure of discs during warps, from 0.5 Gyr before a warp starts to 0.5 Gyr after it ends (for the warps that end before $z = 0$). By doing this, we try to minimize the effect that other processes like mergers may have on the disc, and limit our analysis to the warp only. We first study whether the vertical density structure of the warped region is distinct from the one in the unwarped inner part of the disc. We then follow the time evolution of both the thickness of the disc and the vertical velocity dispersion to understand if the warped region of the disc experiences more vertical heating than the inner disc.

4.1 Inner–outer disc transition

We examine the evolution of the scale heights of the thin disc, thick disc, and mono-age populations during different epochs: before the warp starts (first column of Figs 5 and 6), during the warp (middle columns of Figs 5 and 6), and (when possible) after the warp has ended (last column of Figs 5 and 6). We study whether scale heights behave differently within the warped region of the disc. We find two main cases within our galaxy sample, which are represented in Figs 5 and 6, respectively, and explained below: in the first case, the scale heights never behave very differently within the warped region of the disc. Therefore, in terms of the scale heights, there is no transition between the non-warped and the warped regions of the disc. In the second case, during the warp, the scale heights behave very differently within the warped region of the disc. Hence, there is a transition between the non-warped and the warped regions of the disc in terms of the vertical stellar density.

4.1.1 The vertical density structure is preserved at all times

In this category, we find galaxies whose warps are either internally driven or created by an interaction with a satellite. In those cases, the scale heights of mono-age populations and of the thin and thick disc behave similarly in the inner non-warped region and in the outer warped region of the disc. For instance, in case of a flat thick disc, *top row* of Fig. 5, the scale heights of the thick disc are similar in the inner and outer disc. In case of a flared thick disc, *middle row* and *bottom row* of Fig. 5, the scale heights continuously increase as a function of radius (both for the global thick disc and most of the mono-age populations). The scale heights sometimes flatten slightly in the very outer disc (outside of R_{25}, marked by the dashed black line in Fig. 5), but otherwise they behave similarly in the warped and unwarped regions. It is possible that the similarity between the inner and outer disc might also reinforced by radial migration (Khachaturyants et al. 2021). For the case of **g126** in particular, the flaring displayed in the leftmost panel of the *middle row* is the product of the merger at $t \sim 10.5$ Gyr. Yet, no increase of flaring is observed during the warp's lifetime. In fact, the rest of the panels of the *middle row* show new generations of stars being born in cold and flat configurations also within the warp. Lastly, the *bottom row* of Fig. 5 is also showing that, after the warp is gone, the vertical structure of the disc does not keep a memory of the warp.

It is interesting to notice that warps in this category are created when stellar particles already living in the disc before the warp get tilted. The fact that the geometrical thin/thick disc structure holds without being strongly affected by the warp means that all the stellar particles are shifted uniformly for a given radius and azimuthal region of the disc.

4.1.2 The vertical stellar density is temporarily altered during the warp

In galaxies whose warp is produced by stellar material either being accreted or born in off-plane configurations, the vertical stellar density temporarily changes from the inner and non-warped disc to the outer and warped disc. In particular, during the warp, the warped region of the disc is not well described by a double sech^2 density profile, which in practice leads to large uncertainties on the thick disc scale heights in the warped region (as shown in Fig. 6).

An example of this category is **g39**, which is illustrated in the *top row* of Fig. 6. After a merger at $t \sim 7.5$ Gyr, the vertical density within the disc settles down except close to the disc's edge R_{25} (see

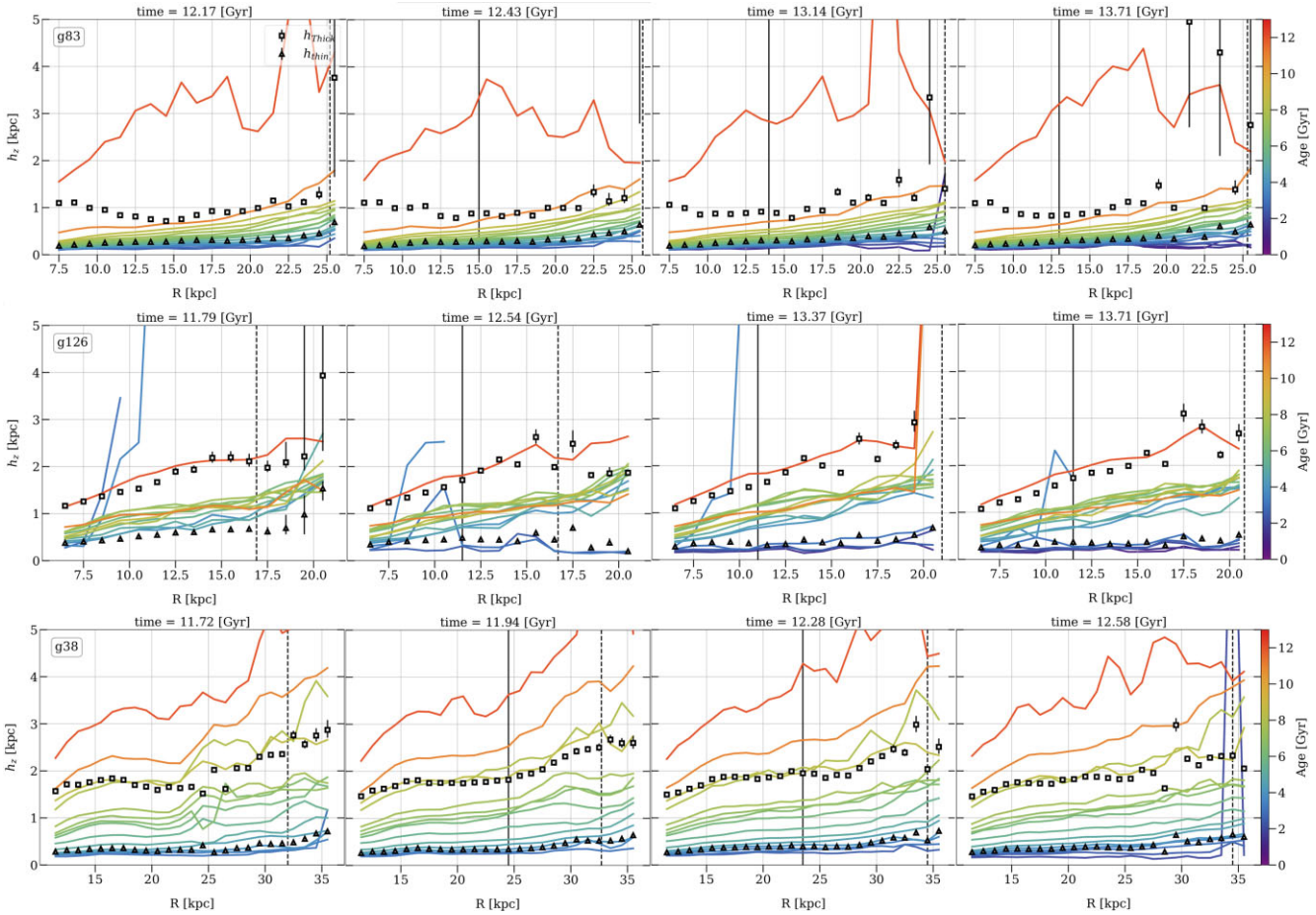

Figure 5. Values of the scale height against radius for the thin disc (triangles), thick disc (squares), and mono-age populations (solid lines) colour-coded by age at $z = 0$. Mono-age populations from 9 to 11 Gyr and from 11 to 13 Gyr are binned together, every other mono-age population spans 0.5 Gyr. The first column corresponds to a time before the start of the warp, the middle columns are during the warp, and the last column is either after the end of the warp, or at $z = 0$. The x-axis spans from the beginning of the disc to R_{25} at the cosmological time of the rightmost panel. The solid vertical black line represents the onset radius of the galactic warp, while the dashed vertical black line marks the value of R_{25} at the time of the snapshot indicated above each panel. The top row represents galaxy **g83**, where the warps starts at 12.3 Gyr and is still in place by $z = 0$. The thick disc stays flat all along. The middle row represents galaxy **g126**, whose warps starts at 12.1 Gyr and is still active by $z = 0$. Both the flaring of the thick disc and MAPs are preserved throughout the warp. The bottom row represents galaxy **g38**, whose warp starts at 11.9 Gyr and fades away at 12.5 Gyr. The scale heights of both thin and thick disc, as well as MAPs do not experience major changes during the warp.

leftmost panel). Later, the warp forms when material spread by the merger is accreted. The amount of material being accreted is such that the stellar vertical density is not well described by a double sech^2 anymore, hence the large uncertainties in the thick disc's scale heights within the warp (see two middle panels). After the warp is gone, the disc settles back into a double sech^2 structure (see rightmost panel).

A similar inner–outer disc transition is observed for galaxies which formed an outer ring structure off-plane, like galaxy **g48** illustrated in the *bottom row* of Fig. 6. At $t \sim 9.7$ Gyr, the disc beyond 14 kpc is poorly described by a double sech^2 (see leftmost panel). This is due to the aftermath of a merger at $t \sim 8$ Gyr, which induced vertical perturbations (although not in the form of a warp). Yet, once the disc recovers from the merger, the double sech^2 structure starts to reappear. A warp then develops in the outer disc because of an interaction with another satellite, leading to the formation of an inclined stellar ring. In this region, the disc structure is altered asymmetrically by the high amount of stellar material at high z above or below the galactic plane (see two middle panels). However, once this material settles down within the disc, the double sech^2 reappears even before the warp is fully gone (see rightmost panel).

Regardless of the accreted/*in situ* origin of the material, warps that fall into this category are created because new material is added to the disc at large height, as opposed to those where stars in the disc get tilted. Here, the double sech^2 structure is not preserved within the warp region, but it reappears after the off-plane material settles down within the disc. As shown in Fig. 6, the reappearance of the double sech^2 is mostly due to the settling down of the warped material rather than to the formation of new stars in an unwarped configuration. Therefore, once the warp is gone, the thin and thick disc structure is recovered, with no sign of where the warp's onset radius used to be.

Here, the double sech2 structure is not preserved within the warp region, but it reappears after the off-plane material settles down within the disc; as shown in Fig. 6, the reappearance of the double sech2 is mostly due to the settling down of the warped material rather than to the formation of new stars in an unwarped configuration.

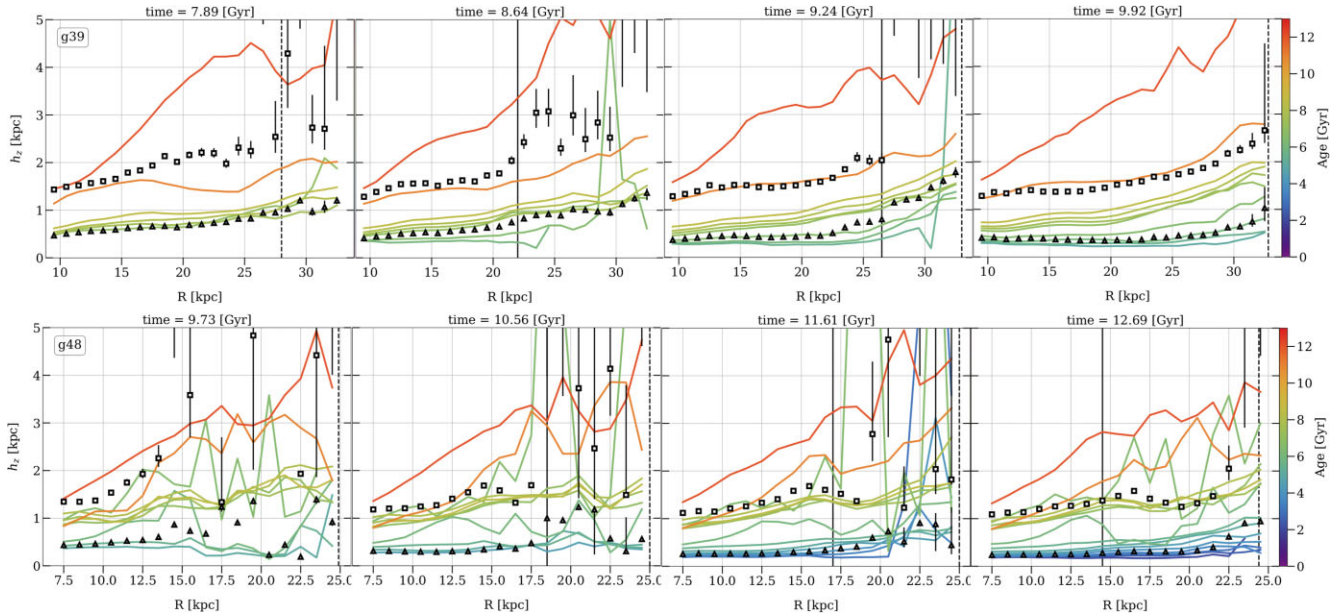

Figure 6. Similar to Fig. 5 but for two galaxies whose disc's vertical density profile is altered during the warps. The top row represents galaxy **g39**, where the warp starts at 8 Gyr and ends at 9.7 Gyr. In the warped region (beyond the solid vertical line), the vertical density structure is no longer well described by a double sech^2, hence the large uncertainties in the thick disc's scale heights. However, as the warp fades away, the global thin/thick disc structure is recovered throughout the disc and no sign of the past warp is seen. The bottom row represents galaxy **g48**, where the warp starts at 9.8 Gyr and is still present at $z = 0$. The same effect can be seen, with the thin and thick disc structure recovered for almost all radii even before the warp has finished.

4.2 Disc heating

In order to clarify whether disc heating or flaring take place during warps, we follow the time evolution of the dispersion of the vertical position and vertical velocity of the stellar particles in two radial bins: one in the inner and non-warped part of the disc, and the other in the outer and warped part of the disc. We monitor the evolution of these quantities only half a Gyr before and after the warp to minimize the effects of other disc heating agents. We only include in the computation stars born before the start of the warp to isolate the effect of the warp on the vertical structure of the disc, and avoid contamination by young stars born during the warp phase.

On the top row of Fig. 7 we show the dispersion of the vertical position in a region within the inner disc (*top*) and outer disc (*bottom*). Clearly, the disc thickness does not change as a function of time for most galaxies, both in the inner and outer region of the discs. The two cases where there is a significant change are **g48** and **g59**. For these galaxies, which have long-lasting warps, the inner disc actually becomes thinner with time (even when only considering stars born before the start of the warp), because of the gravitational influence of new generations of stars being born in a cold configuration.

A similar effect is observed on the bottom row of Fig. 7. The vertical velocity dispersion does not increase because of the warp (both in the inner and outer disc). In many cases, the vertical velocity dispersion does not change at all. In a few cases, we see σ_{v_z} decrease because of response of the disc to the formation of young stars in a cold configuration.

From this, we conclude that disc heating does not happen during warps, even in the outer regions. This can be due to a few different reasons. First, in cases of warps triggered by interactions, we find that heating happens on faster time-scales than warping: warps need a few dynamical time-scales to fully emerge. This means that disc heating is finished before the warp starts to dominate the structure of the disc. The best example of this is galaxy **g126** in the *middle row* of Fig. 5: a merger happens at $t \sim 10.5$ Gyr and creates flaring before the warp starts at $t \sim 12.1$ Gyr (see leftmost panel of *middle row* of Fig. 5). Then, the warp develops and no further heating or flaring is observed. Second, not all galaxy–satellite interactions may cause vertical disc heating as pointed out by Velázquez & White (1999). In particular, most of the interactions responsible for warps in our simulations have very small mass ratios: except for g126, all galaxies undergo interactions with mass ratios between 1:20 and 1:70. Those small interactions are enough to create strong warps, but not to heat discs vertically (see for instance Moetazedian & Just 2016). Finally, while Khoperskov et al. (2010) and Griv (2011) suggested that bending waves can cause vertical disc heating, we find that warps are not a source of vertical heating in our simulations. It could be that in a few galaxies the lack of heating might be connected to a saturation effect (e.g. Quillen & Garnett 2001). However, we find that even galaxies with a low velocity dispersion do not experience heating during warps (see Fig. 7), so saturation cannot explain the general lack of heating we observe in all galaxies. Thus, warps only correspond to a global shift of the vertical structure of the disc or to an asymmetrical alteration of the vertical density, and when warps disappear discs recover their initial vertical structure. It is unclear where the energy that excited a warp is transferred after the warp fades: this remains to be explored in future work.

5 CONCLUSIONS

In this work, we analysed the connection between disc heating and warping using the simulations from Martig et al. (2012). We chose a subsample of six simulated galaxies with warps present at $z = 0$, as well as five other galaxies which underwent warps in the past. We computed scale heights for mono-age populations as well as for thin and thick discs after correcting for the warps' vertical shift as explained in Section 2 and represented in Fig. 3.

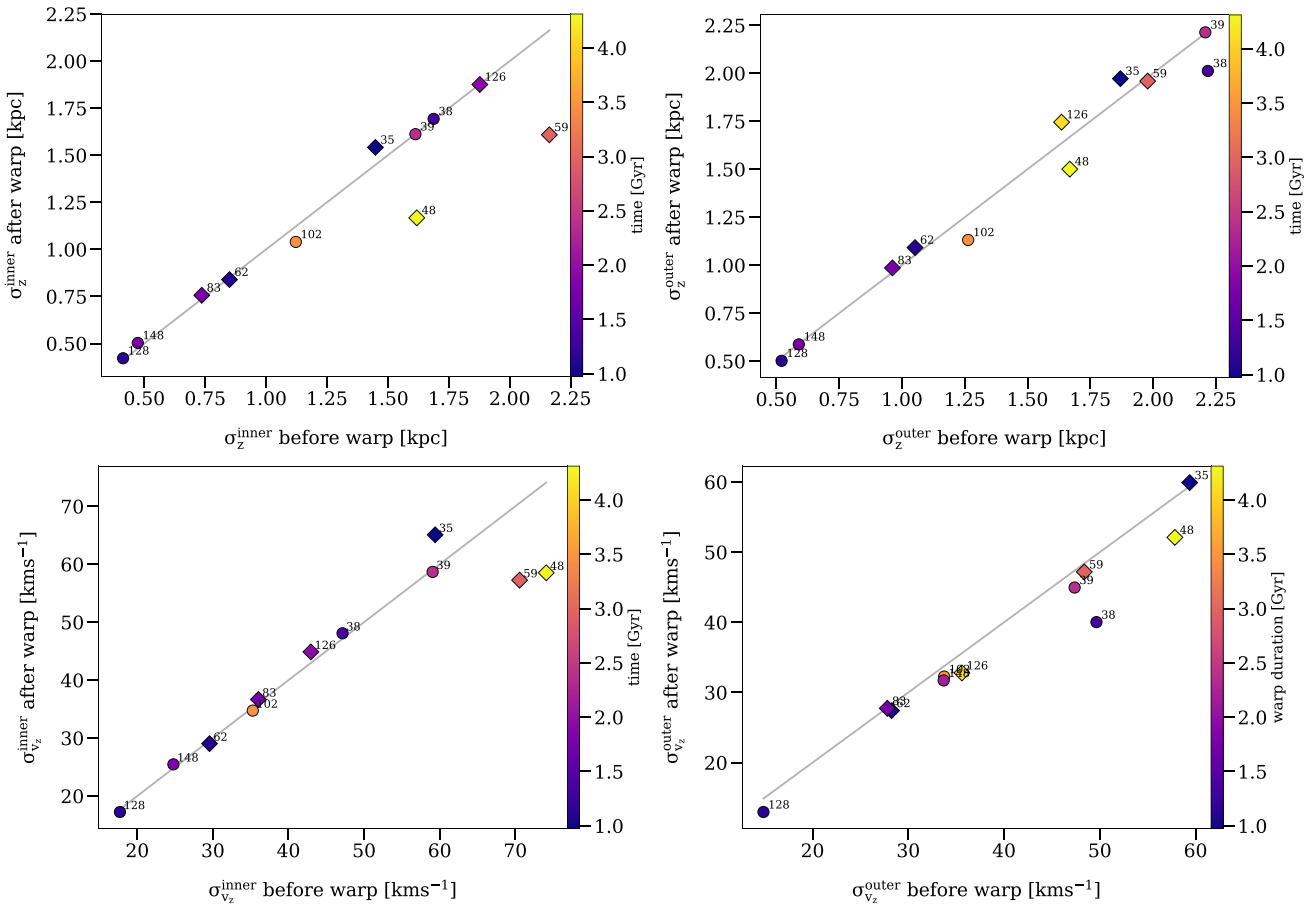

Figure 7. *Top row:* standard deviation of the vertical position of the stellar particles before and after the warp within a region in the non-warped part of the disc (left), and outer and warped part of the disc (right). Points are colour-coded by the duration of the warp, and the shape represents whether the warp is finished (circles) or not (diamonds). We only include in the computation stars born before the start of the warp to isolate the effect of the warp on the vertical structure of the disc. *Bottom row*: equivalent of the top row for the vertical velocity dispersion. These plots show that there is no disc heating during the warp. For most galaxies, both the disc thickness and the vertical velocity dispersion are nearly constant as a function of time, even when we only consider populations born before the start of the warp.

We found that for warps either internally driven or created by interactions, the scale heights of the geometrical thin and thick disc, and of mono-age populations, are not affected by the warp: whether the thin and thick disc are flat or flared, the trend is always preserved all the way through the disc. In other words, for warps formed when the stars are shifted off-plane, the warp seems to affect uniformly all the stellar disc, and does not alter the structure of the vertical stellar density. We also noted that these warps tend to have shorter lifetimes and reach lower heights above/below the galactic plane.

On the other hand, galaxies whose warps are created by the accretion or the formation of stars in off-plane configurations show a vertical stellar density structure that temporarily changes between the inner and non-warped region of the disc and the warped one. While the non-warped region keeps having a double sech^2 density profile, this is altered asymmetrically in the warped region due to the off-plane material. However, once the warp fades away, the double sech^2 is recovered and the trends of the thin/thick disc scale heights as well as of mono-age populations are coherent throughout the disc, without a signature of a pre-existing warp. Additionally, these warps tend to last longer and reach larger heights above/below the galactic plane than the others.

Finally, we found that for all warps the disc thickness and the vertical velocity dispersion do not increase during the warp, indicating that there is no disc heating happening during warps. This can be either because the disc heating induced by the warp agent takes place before warp formation, or because neither the warp agent nor the warp itself is a source of disc heating.

Our results suggest that depending on their origin, warps may or may not alter the vertical stellar structure of the stellar disc. Nevertheless, once warps disappear, they do not leave any imprint in the stellar populations living in the disc. Therefore, in terms of stellar vertical density structure and vertical heating in the disc, galaxies do not hold any memory of warps they might have experienced in the past. Given the relatively small size of our galaxy sample, further work using larger samples from different simulations would greatly help confirm these results.

ACKNOWLEDGEMENTS

We thank Phil James for his support and for useful discussions. We would like to acknowledge a LIV.DAT doctoral studentship supported by the STFC under contract ST/P006752/1. The LIV.DAT Centre for Doctoral Training (CDT) is hosted by the University of Liverpool and Liverpool John Moores University/Astrophysics Research Institute.

DATA AVAILABILITY

The data underlying this article will be shared on reasonable request to the corresponding author.

REFERENCES

Alfaro E. J.., Perez E., Gonzalez Delgado R. M., Martos M. A., Franco J., 2001, ApJ, 550, 253
Amôres E. B., Robin A. C., Reylé C., 2017, A&A, 602, 67
Ann H. B., Park J. C., 2006, New Astron., 11, 293
Antoja T. et al., 2018, Nature, 561, 360
Antoja T. et al., 2021, A&A, 649, 115
Aumer M., White S. D., 2013, MNRAS, 428, 1055
Battaner E., Jiménez-Vicente J., 1998, A&A, 332, 809
Battaner E., Florido E., Sanchez-Saavedra M., 1990, A&A, 236, 1
Bennett M., Bovy J., 2019, MNRAS, 482, 1417
Bosma A., 1981, AJ, 86, 1825
Bournaud F., Combes F., 2002, A&A, 392, 83
Bournaud F., Combes F., 2003, A&A, 401, 817
Bournaud F., Elmegreen B. G., Martig M., 2009, ApJ, 707, L1
Chen X., Wang S., Deng L., de Grijs R., Liu C., Tian H., 2019, Nat. Astron., 3, 320
Cheng X. et al., 2020, ApJ, 905, 49
Chequers M. H., Widrow L. M., 2017, MNRAS, 472, 2751
Debattista V. P., Sellwood J. A., 1999, ApJ, 513, L107
Faure C., Siebert A., Famaey B., 2014, MNRAS, 440, 2564
Foreman-Mackey D., Hogg D. W., Lang D., Goodman J., 2013, PASP, 125, 306
Garavito-Camargo N., Besla G., Laporte C. F. P., Johnston K. V., Gómez F. A., Watkins L. L., 2019, ApJ, 884, 51
García de la Cruz J., Martig M., Minchev I., James P., 2021, MNRAS, 501, 5105
García-Ruiz I., Sancisi R., Kuijken K., 2002, A&A, 394, 769
Gerssen J., Shapiro Griffin K., 2012, MNRAS, 423, 2726
Gómez F. A., Minchev I., O'Shea B. W., Beers T. C., Bullock J. S., Purcell C. W., 2013, MNRAS, 429, 159
Gómez F. A., White S. D., Grand R. J., Marinacci F., Springel V., Pakmor R., 2017, MNRAS, 465, 3446
Gómez F. A. et al., 2021, ApJ, 908, 27
Griv E., 2011, MNRAS, 415, 1259
Heald G. et al., 2011, A&A, 526, A118
Hunt J. A. S., Stelea I. A., Johnston K. V., Gandhi S. S., Laporte C. F. P., Bedorf J., 2021, MNRAS, 508, 1459
Ideta M., Hozumi S., Tsuchiya T., Takizawa M., 2000, MNRAS, 311, 733
Jiang I. G., Binney J., 1999, MNRAS, 303, L7
Jungwiert B., Combes F., Palous J., 2001, A&A, 376, 85
Kazantzidis S., Bullock J. S., Zentner A. R., Kravtsov A. V., Moustakas L. A., 2008, ApJ, 688, 254
Kazantzidis S., Zentner A. R., Kravtsov A. V., Bullock J. S., Debattista V. P., 2009, ApJ, 700, 1896
Kennicutt R. C., Jr, 1998, ApJ, 498, 541
Khachaturyants T., Beraldo e Silva L., Debattista V. P., 2021, MNRAS, 508, 2350
Khoperskov A., Bizyaev D., Tiurina N., Butenko M., 2010, Astron. Nachr., 331, 731
Kim J. H., Peirani S., Kim S., Ann H. B., An S. H., Yoon S. J., 2014, ApJ, 789, 90
Laporte C. F. P., Gómez F. A., Besla G., Johnston K. V., Garavito-Camargo N., 2018, MNRAS, 473, 1218
Laporte C. F. P., Minchev I., Johnston K. V., Gómez F. A., 2019, MNRAS, 485, 3134
Levine E. S., Blitz L., Heiles C., 2006, ApJ, 643, 881
Liu C., Tian H. J., Wan J. C., 2016, Proc. IAU Symp. Vol. 321, The Age-Kinematical Features in the Milky Way Outer Disk. Kluwer, Dordrecht, p. 611
López-Corredoira M., Molgó J., 2014, A&A, 567, A106
López-Corredoira M., Cabrera-Lavers A., Garzón F., Hammersley P. L., 2002, A&A, 394, 883
López-Corredoira M., Prieto C. A., Garzón F., Wang H., Liu C., Deng L., 2018, A&A, 612, L8
Martig M., Bournaud F., 2010, ApJ, 714, L275
Martig M., Bournaud F., Teyssier R., Dekel A., 2009, ApJ, 707, 250
Martig M., Bournaud F., Croton D. J., Dekel A., Teyssier R., 2012, ApJ, 756, 26
Martig M., Minchev I., Flynn C., 2014, MNRAS, 443, 2452
Minchev I., Martig M., Streich D., Scannapieco C., De Jong R. S., Steinmetz M., 2015, ApJ, 804, L9
Moetazedian R., Just A., 2016, MNRAS, 459, 2905
Narayan C. A., Dettmar R. J., Saha K., 2020, MNRAS, 495, 3705
Ostriker E. C., Binney J. J., 1989, MNRAS, 237, 785
Pinna F., Falcón-Barroso J., Martig M., Martínez-Valpuesta I., Méndez-Abreu J., van de Ven G., Leaman R., Lyubenova M., 2018, MNRAS, 475, 2697
Poggio E. et al., 2018, MNRAS, 481, L21
Poggio E., Laporte C. F. P., Johnston K. V., D'Onghia E., Drimmel R., Grion Filho D., 2021, MNRAS, 508, 541
Purcell C. W., Bullock J. S., Tollerud E. J., Rocha M., Chakrabarti S., 2011, Nature, 477, 7364
Quillen A. C., Garnett D. R., 2001, in Funes J. G., Corsini E. M., eds, ASP Conf. Ser. Vol. 230, Galaxy Disks and Disk Galaxies. Astron. Soc. Pac., San Francisco, p. 87
Reshetnikov V., Combes F., 1998, A&A, 337, 9
Reshetnikov V. P., Mosenkov A. V., Moiseev A. V., Kotov S. S., Savchenko S. S., 2016, MNRAS, 461, 4233
Revaz Y., Pfenniger D., 2004, A&A, 425, 67
Romero-Gómez M., Mateu C., Aguilar L., Figueras F., Castro-Ginard A., 2019, A&A, 627, 150
Roškar R., Debattista V. P., Brooks A. M., Quinn T. R., Brook C. B., Governato F., Dalcanton J. J., Wadsley J., 2010, MNRAS, 408, 783
Saha K., Jog C. J., 2006, A&A, 446, 897
Sánchez-Gil M. C., Alfaro E. J., Pérez E., 2015, MNRAS, 454, 3376
Sánchez-Saavedra M. L., Battaner E., Guijarro A., López-Corredoira M., Castro-Rodríguez N., 2003, A&A, 399, 457
Sancisi R., 1976, A&A, 53, 159
Scannapieco C., White S. D., Springel V., Tissera P. B., 2009, MNRAS, 396, 696
Schwarzkopf U., Dettmar R. J., 2001, A&A, 373, 402
Sellwood J. A., Nelson R. W., Tremaine S., 1998, ApJ, 506, 590
Semczuk M., Lokas E. L., D'Onghia E., Athanassoula E., Debattista V. P., Hernquist L., 2020, MNRAS, 498, 3535
Shen J., Sellwood J. A., 2006, MNRAS, 370, 2
Sparke L. S., Casertano S., 1988, MNRAS, 234, 873
Teyssier R., 2002, A&A, 385, 337
Thomas G. F. et al., 2018, MNRAS, 481, 5223
Toth G., Ostriker J. P., 1992, ApJ, 389, 5
Urrejola-Mora C., Gómez F. A., Torres-Flores S., Amram P., Epinat B., Monachesi A., Marinacci F., Mendes de Oliveira C., 2022, ApJ, 935, 20
Van Der Kruit P. C., 2007, A&A, 466, 883
Van Der Kruit P., Searle L., 1981, A&A, 95, 105
Velázquez H., White S. D., 1999, MNRAS, 304, 254
Vesperini E., Weinberg M. D., 2000, ApJ, 534, 598
Villalobos A., Helmi A., 2008, MNRAS, 391, 1806
Virtanen P. et al., 2020, Nat. Methods, 17, 261
Weinberg M. D., 1998, MNRAS, 299, 499
Weinberg M. D., Blitz L., 2006, ApJ, 641, 33
Yu Y. et al., 2021, ApJ, 922, 80
Yurin D., Springel V., 2015, MNRAS, 452, 2367

APPENDIX: FORMATION OF AN INCLINED STELLAR RING

In Fig. A1, we show the formation of an inclined outer stellar ring to have a visual clarification of the process explained in Section 3.4. The galaxy shown here is galaxy **g48**.

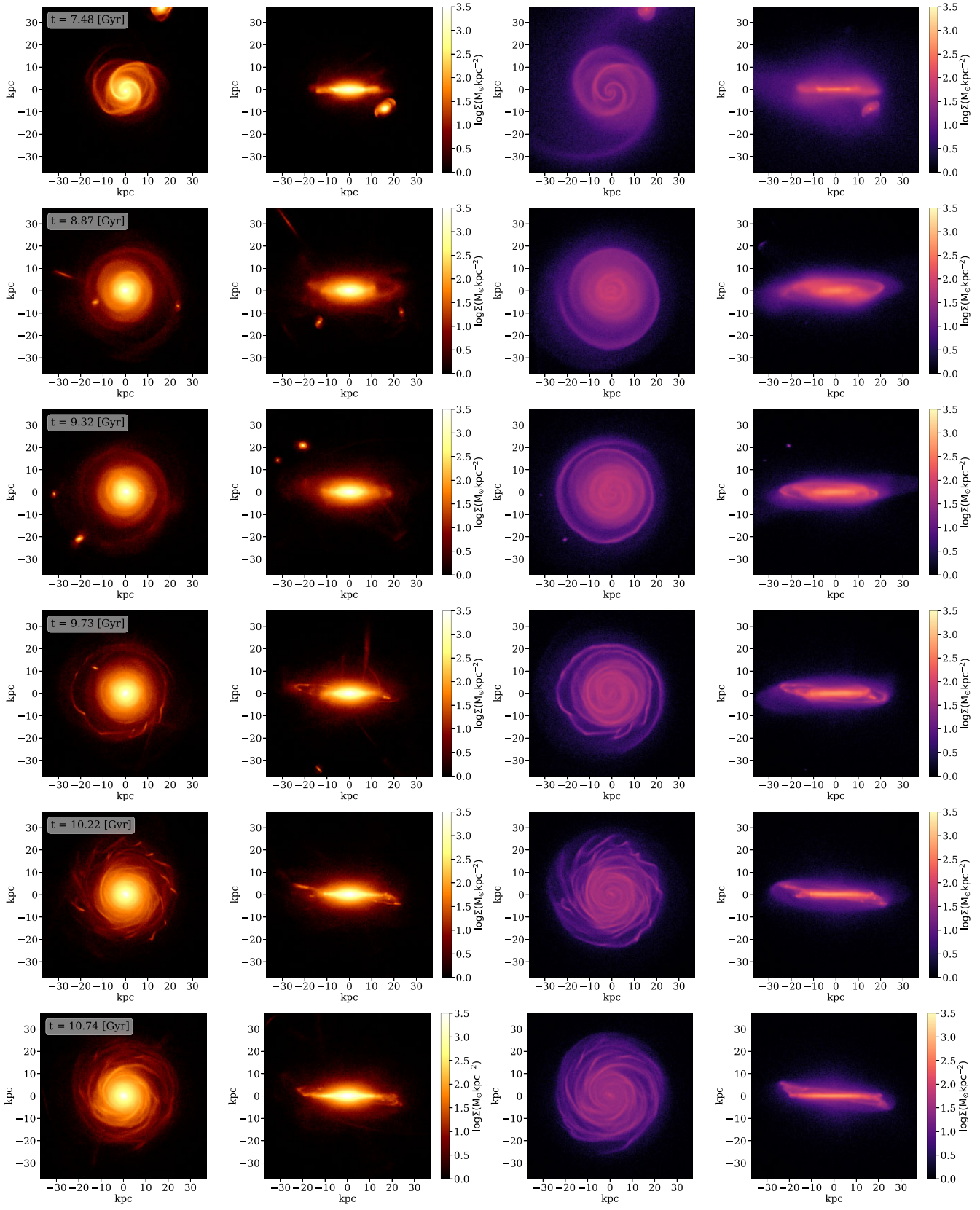

Figure A1. On the two left columns are stellar density maps of galaxy **g48** seen face-on and edge-on. On the two right columns are gas density maps of the galaxy seen face-on and edge-on. The first row from the top shows the moment before the merger of the satellite. The second row shows the aftermath of the merger, with the stellar but especially the gas disc being off-plane. The third row shows the moment the satellite flies by. On the fourth and fifth rows, the stellar ring forms and starts to break. Finally, on the bottom row, the stellar ring has merged with the outer disc and the warp is fully formed.

This paper has been typeset from a TEX/LATEX file prepared by the author.